# Numerical Study of Liquid Film Formation around Tubes of Horizontal Falling Film Evaporator

A. Kumar Poddar[†] and N. K. Singh

*National Institute of Technology, Kurukshetra, Haryana, 136119, India*

†*Corresponding Author Email:er.awadhesh2010@gmail.com*

## ABSTRACT

Falling film evaporative heat exchangers are extensively used in processing industries; broad areas of application being refrigeration, desalination and food processing industries. The fundamental aspect of this type of heat transfer process is to extract the process heat in the form of latent heat by liquid which is sprayed over the surface of the process tubes. Formation of liquid film over a fully wetted horizontal round tube of falling film evaporator has been numerically simulated here. Two numerical approaches, Volume of Fluid (VOF) technique and the Eulerian multiphase model are applied to compare their results. The effect of varying flow and geometrical parameters on the film thickness is investigated. Two horizontal tubes of diameter 19.05mm and 25.04mm with three different uniform spacing have been selected for simulation. Film Reynolds numbers 650, 950 and 1250 are considered for the above set of parameters. Ii is observed that the geometrical and flow parameters considerably influence the film thickness. Transient analysis of the film formation has been carried out and parameters like pathline of liquid film and the velocity profile have been obtained for understanding the flow behavior in a better manner. All the simulated results agree well with the published data.

Keywords: CFD; Horizontal round tube; Liquid film thickness; Volume of fluid method; Eulerian multiphase model.

## NOMENCLATURE

| | | | |
|---|---|---|---|
| B | circumferential Angle | $v$ | velocity in y-direction |
| D | diameter of tube | | |
| G | gas | α | volume fraction |
| *g* | *gravitational acceleration* | Λ | column spacing |
| L | liquid | δ | film thickness |
| P | Pressure | $\rho$ | density of fluid |
| S | tube spacing | $\Gamma$ | film flow rate |
| *u* | velocity in x-direction | $\tau$ | shear stress |
| μ | viscosity of fluid | | |

## 1. INTRODUCTION

Falling film evaporative heat exchangers contribute significantly to effective utilization of energy transformation processes. The modern heat exchangers need to be very efficient and many times are to be operated at very small temperature gradients. This requirement is well fulfilled by evaporative heat exchanger which is able to operate with low grade energy and can be operated at very low temperature gradient. These features make it superior in energy saving as well as environment protection. Many industries like food processing plants, desalination plants etc. use falling film evaporative heat exchangers. Figure 1 shows the working process of falling film evaporators. Continuous research is going on to improve the performance of evaporative heat exchangers through experimental, analytical as well as simulation approaches. The main carrier of heat transfer in falling film evaporative heat exchangers is the film formed around the tube surface. The heat transfer and mass diffusion processes are affected by the thickness of film around the outer

circumferences of the processing tube. The optimized uniform liquid film thickens contributes to a major role in heat exchange process. Study of liquid film distribution and tube alignment are the effective methods for prediction of the uniformity in heat transfer process and finding out the possible places of dry patch formation. At very low Reynolds numbers the liquid film thickness reduces sharply and possibility of formation of dry patches increases whereas at very high Reynolds number liquid film thickness increases so the evaporation phenomenon get reduced and the heat transfer process decreases sharply so it is important to optimize the process with the performance parameters like Reynolds number, tube spacing and their alignments. A remarkable analytical investigation was carried out by Nusselt (1916). He suggested the classical expression (Eq. 1) to get the liquid film thickness around the outer surface of fully wetted horizontal tube.

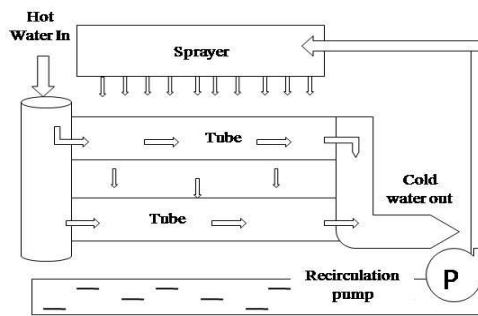$$\delta = \left( \frac{3\mu_L \Gamma}{\rho_L (\rho_L - \rho_G) g \sin \beta} \right)^{\frac{1}{3}} \quad (1)$$



**Fig. 1. Falling film evaporator.**

This classical expression assumes a continuous sheet mode of flow and also neglects the momentum effect. Figure 2 schematically shows the mechanism of flow in falling film evaporative heat exchangers on a single tube. A continuous mode of liquid flow over the tube surface interacts with the heated tube and heat transfer occurs from the tube surface to liquid film. Some fraction of mass gets evaporated from liquid film after getting heat from the tube surfaces. The remaining liquid continues to flow downward due to gravity free fall conditions. Thus heat transfer is governed by two mechanisms, first the transferring of latent heat to the liquid film so that it converted into vapors and the then convection heat transfer process with the flowing fluid.

Three types of flows are distinguished to classify the mode of flow (Fig. 3):

Droplet mode: - In droplet mode, the flow appears between the tubes in droplet form.

Column mode: - In column mode, the flow exists in liquid columns in between the tubes.

Sheet mode: - In the sheet mode, the flow appears continuous. This mode of flow is of great interest

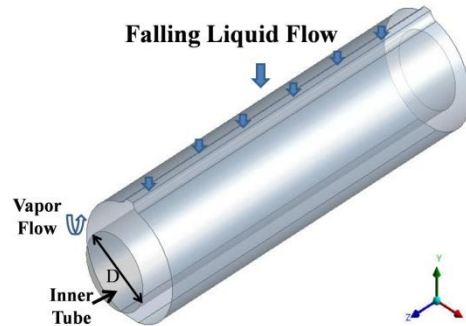among the researchers and has been investigated thoroughly.



**Fig. 2. Mechanism of flow.**

A non-contact film thickness measurement technique was used by Dukler et al. (1952) in their experiment. They used a capacitance method to detect the film thickness. The film thickness of falling liquid flows over a horizontal round tube has been extensively investigated by Rogers and Goindi (1989). They mounted a dial point gauge at 45º, 90ºand 135º circumferential locations to find out the film thickness and they found that the value measured by them is 30% greater than the Nusselt values.
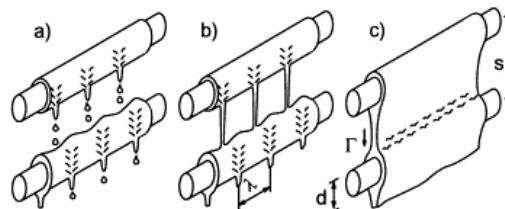


**Fig. 3. Flow Modes (a) Droplet, (b) Column, (c) Sheet (Armbruster and Mitrovic, 1998).**

Now an optical method is extensively used to measure the thickness of the liquid film. Zhang et al. (2000) captured the images from a video camera to find out the average film thickness on a vertical tube.

A laser induced fluorescence technique to detect the interface of liquid film was used by Desevaux et al. (2002). Wang et al. (2009, 2010) investigated experimentally to find out the film thickness for Turbo-CII tube and for plain tube. They investigated it for different tube spacing and different flow rates. They found very little variation and results were almost similar in nature while using Turbo-CII and plain tube. In their experiments the flow patterns were also well quantified by using working fluid as water and ethylene glycol. An experimental investigation was carried out by Hou et al. (2012), for measuring the film thickness by using displacement micrometer. They observed that the film Reynolds number, intertube spacing, and diameter of tube affect the distribution characteristics. They also suggested a correlation on the basis of Nusselt correlation in the

specified range of their experimental investigation.

A laser measurement technique was also investigated by Gstoehl *et al.* (2004) to get the film thickness and they concluded that on the lower circumferential portion of the tube the Nusselt falling film theory gives an overestimate. Three horizontal test tubes are arranged in a vertical array and liquid flows under gravity free fall condition over it. Laser-induced fluorescence and laser tomography techniques were used for visualization of flow. Similar experiments were conducted by Ribatski and Thome (2007), Christians *et al.* (2012) and Anglart *et al.* (2015). Wunder *et al.* (2017) numerically investigated heat transfer in a horizontal falling film evaporator of multiple-effect distillation. Their observation is that the film thickness plays a major role in formation of dry patches and strongly affects the coefficient of heat transfer in falling film heat transfer process. Chen *et al.* (2015) simulated the pattern of falling film on a horizontal tube bundle of falling film evaporator. A Volume of Fluid (VOF) technique was used by them for tracking the free surface of two phase flow. This mathematical model was well validated by experimental results. A copper tube of smooth surface was chosen for simulation. They observed that the flow mode changes from droplet mode to droplet-columnar mode, and columnar mode of flow to columnar-sheet mode of flow and the last is sheet mode of flow patterns with varying flow rates.

Ji *et al.* (2016) experimentally observed that the flow rate of liquid film is an important parameter which influences the evaporating heat transfer coefficient. The vapor flow and its positive as well as negative effects were extensively investigated. In their study, falling film heat transfer coefficients are measured with different heat fluxes. Lee *et al.* (2019) studied the liquid film distribution on elliptical tube to get the heat transfer characteristics by varying the flow rate and dispense angle. They observed that at low flow rates the liquid is unable to envelop the entire tube surface. They suggested a normal range of flow rate under which a good thermal performance can be achieved.

## 2. NUMERICAL INVESTIGATION

Tube arrays are arranged horizontally with equal spacing between them. To minimize the computational time, a symmetry condition is to be considered for half of the solution domain. It is shown in Fig. 4.

The mesh views are shown in Fig. 5. The working fluid is taken as water, which is incompressible and has a very low viscosity. A predetermined volume of mass flow passes over the entire surface of the tube enveloping a thin liquid film over it. The properties of the working fluid are not changing during the process and normal temperature and pressure are to be considered during the process. Inflation technique has been used near the wall surfaces to capture small changes in the fluid behavior around the surface of the tube.
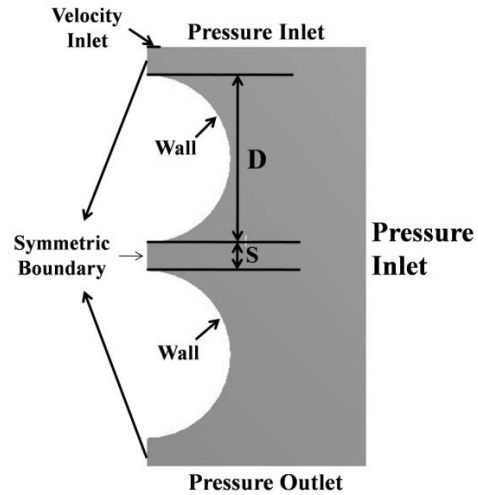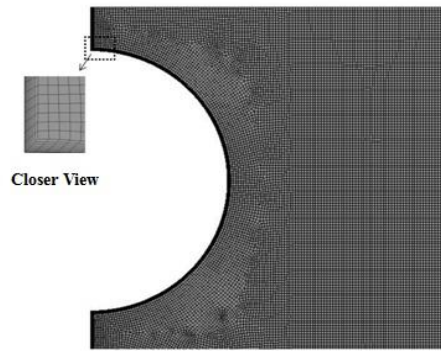

**Fig. 4. Simulation domain.**


**Fig. 5. View of the mesh.**

Top portion of the solution domain is divided into two portions, one portion is selected as velocity inlet boundary condition and rest is considered as pressure inlet boundary condition. The surface of tube wall is considered to be smooth and no slip boundary condition is to be considered without any heat flux. Pressure inlet boundary condition is used on the right side of the solution domain and the bottom of the solution domain is selected as pressure outlet boundary condition for CFD simulation.

## 3. COMPUTATIONAL APPROACH

Continuity equation, momentum equation, and material equations are the fundamental equations to be used to solve the problem. A conservation of material equation with volume fraction method is also used for finding out the film thickness. A comparative study has been done to distinguish the interface of phases with Volume of Fluid (VOF) and Eulerian multiphase methods. Partial differential equations are solved explicitly with a finite volume approach. Navier-Stokes equations have been solved by using Pressure Implicit with Splitting of Operator (PISO) method. For getting the interface between liquid and air, a Geometric Reconstruction Scheme is applied. For complete wetting of the surface of the tube, the wall contact angle is taken to be zero and the simulation is

performed under purely adiabatic condition. In the primary stage, the solution domain is assumed to be filled with air for which the volume fraction ($\alpha_G$) is taken to be zero and volume fraction of water ($\alpha_L$) is taken as one. Water is considered as secondary fluid and fills the solution domain thereafter. Film Reynolds number of cooling water is determined as $Re_f = 4\Gamma/\mu$, where $\Gamma$ is the liquid film flow rate per unit wetted perimeter. Numerical simulations have been performed for fixed diameters with variable Reynolds numbers and also with different tube spacing. Grid independence test plays an important role in CFD simulation. This test ensures that the solution accuracy does not depend on the number of grid points chosen for simulation. Grids with number of nodes 16586, 19884, 21564, 23654, 26558, 29572 and 33569 are used for the grid independence test. Figure 6 shows the thickness calculated at 90° location with different number of nodes.
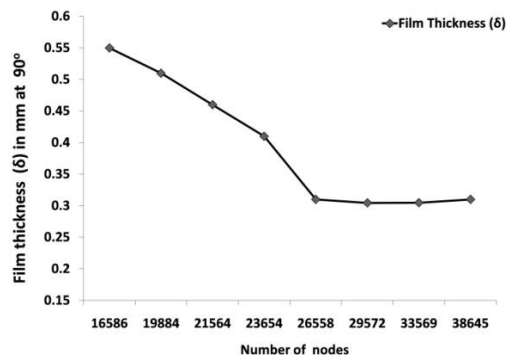


**Fig. 6. Grid independence test.**

The tube diameter (D = 19.05) and spacing (S =6.4) are kept constant during grid independence test. An optimized value of 26558 nodes is found satisfactory for this investigation. For maintaining a consistent level of accuracy in transient flow process a variable time step has been considered. Surface tension for air and water is to be taken as constant (0.072N/m) in VOF model.

Governing equations to be used in simulation are:
Conservation of mass equation:

$$\frac{\partial \rho}{\partial t} + \nabla \cdot (\rho \vec{V}) = 0 \qquad (2)$$

Momentum equation:

X- Component:

$$\frac{\partial(\rho u)}{\partial t} + \nabla \cdot (\rho u \vec{V}) = -\frac{\partial p}{\partial x} + \frac{\partial \tau_{xx}}{\partial x} + \frac{\partial \tau_{yx}}{\partial y} + \rho f_x \quad (3)$$

Y- Component:

$$\frac{\partial(\rho v)}{\partial t} + \nabla \cdot (\rho v \vec{V}) = -\frac{\partial p}{\partial y} + \frac{\partial \tau_{xy}}{\partial x} + \frac{\partial \tau_{yy}}{\partial y} + \rho f_y \quad (4)$$

Material Equation:

$$\frac{\partial(\alpha)}{\partial t} + \vec{v} \cdot \nabla \alpha = 0 \qquad (5)$$

Volume Fraction:

$$\rho = \alpha_l \rho_l + \alpha_G \rho_G \qquad (6)$$
$$\mu = \alpha_l \mu_l + \alpha_G \mu_G \qquad (7)$$

## 4. RESULT AND DISCUSSION

### 4.1 Validation of Numerical Methods

The simulated results are compared with the correlation of Nusselt (1916) and with experimental results of Gstoehl *et al.* (2004) and found to be in good agreement. Film thickness first decreases and after attaining minimum thickness it starts increasing; a similar trend has been found in simulated results. Two set of parameters with tube diameter 19.05mm have been taken at tube spacing 6.4mm & 9.5mm. Two different numerical methods, volume of fluid (VOF) and Eulerian multiphase model are applied and the nature of the results obtained from them are very similar.

The liquid film thickness variations are determined at 20° intervals which is shown in Fig. 07. The impingement zone exists in the interval of 0° to 20°, in this region, the film thickness is very irregular in nature therefore it was not taken into consideration.

After the impingement zone normal behavior of flow begins. Both the results agree well with the earlier experimental results reported by researchers. A comparative study has been shown in Fig. 8. (a) & Fig. 8. (b). Numerical simulation captures all the flow behavior in the given conditions. The film thickness is continuously decreasing until it attains its minimum thickness, after that it starts increasing upto the lower stagnation point of the tube.

### 4.2 Effect of Reynolds Number and Tube Spacing on Film Thickness

Film thickness on horizontal round tubes is strongly influenced by film Reynolds number and tube spacing. The variation of film thickness for different film Reynolds numbers (Re = 650, 950, & 1250) and intertube spacing (S = 3.2mm, 6.4mm, & 9.5mm) for two different diameters of tubes (D = 19.05mm & 25.04mm) is investigated here.

At the impingement zone of the tube, the free falling fluid first comes to rest and then due to inertial effect, it starts moving around the tube. At the center of impingement zone the stagnation zone forms where the fluid comes to rest and hence the film thickness attains its maximum value near the stagnation zone of the tube. This phenomenon is clearly observed in all the cases of investigation.

Hou *et al.* (2012) also had similar observations in this zone. After leaving the stagnation zone, the film thickness starts decreasing and reaches its minimum value around $110^0$ to $140^0$, at this location the velocity of the film attains its maximum value and then thickness starts increasing; it continues to increase upto the bottom of the tube. Film thickness around the circumference of the tube has been investigated with two set of parameters. First set of parameters (D =19.05; S = 3.2, 6.4, 9.5; $Re_f$ = 650, 950, 1250) and another set of parameters
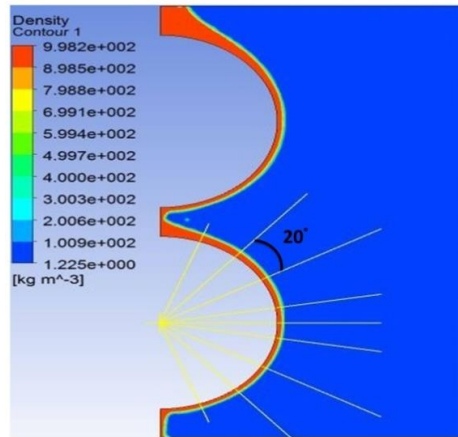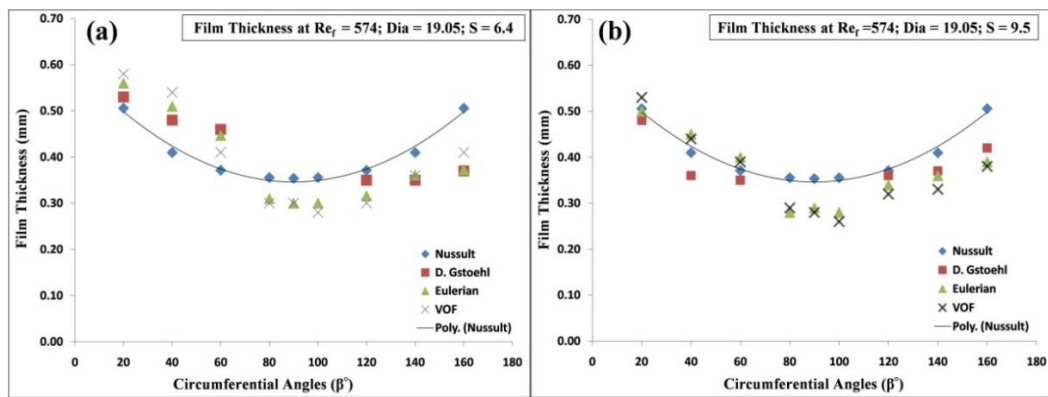
**Fig. 7. Distribution of intervals at 20°.**



**Fig. 8. Comparison of film thickness distribution (a) Re$_f$ =574; D = 19.05; S = 6.4 (b) Re$_f$ =574; D = 19.05; S = 9.5.**

(D =25.04; S = 3.2, 6.4, 9.5; Re$_f$ = 650, 950, 1250) are depicted on separate figures (Fig. 9. and Fig. 10).



**Fig. 9. Film thickness variation with circumferential angle (D = 19.05).**

The location of minimum thickness is slightly shifted towards the lower side of the tube. As the film Reynolds number increases from 650 to 950 and to 1250, the behavior of liquid flow become stream lined and flow of liquid takes place in an organized manner. Also when the tube spacing

changes from S = 3.2mm to S = 6.4mm the flow is again streamlined for the film Reynolds numbers (950, and 1250). The film thickness continues to show an unpredictable behavior at film Reynolds number 650 for both the diameter of the tubes.
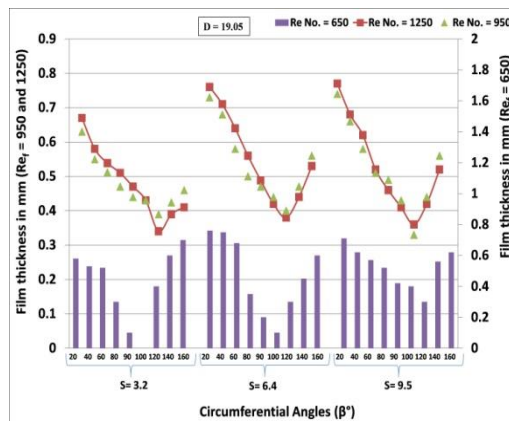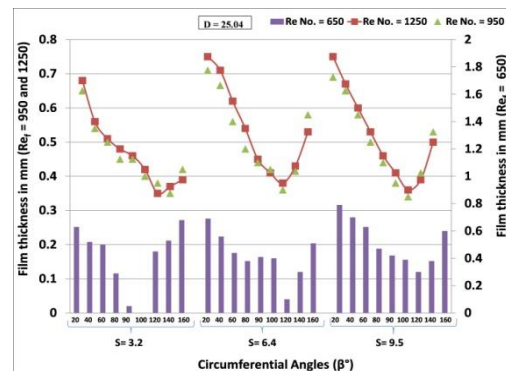


**Fig. 10. Film thickness variation with circumferential angle (D= 25.04)**

A marginal variation in film thickness is recorded when the tube spacing increases to 9.5mm for both tube diameters. The film thickness is greater at low Reynolds number on the upper side of the tube and it decreases sharply as compared to other set of
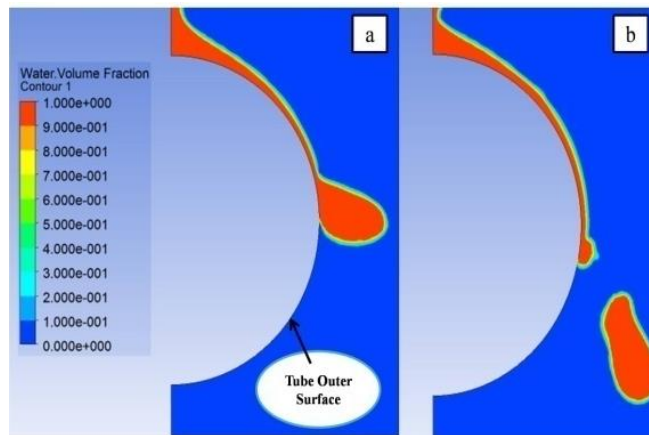
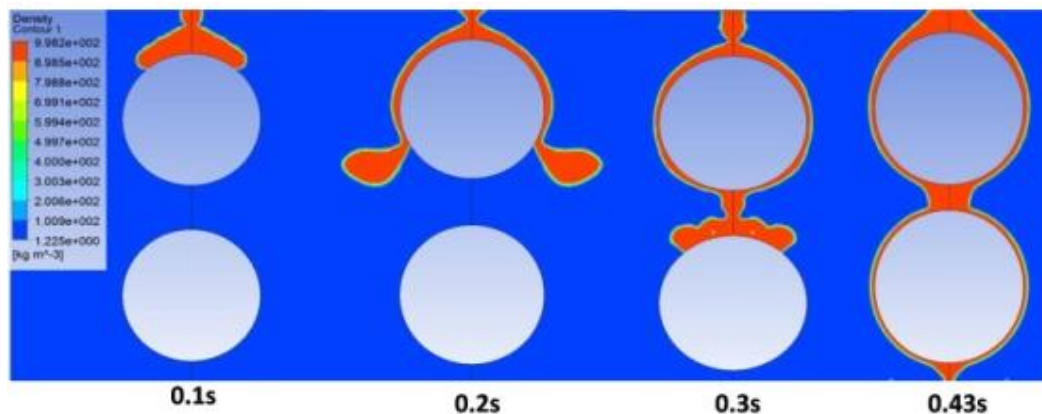**Fig. 11. Mass accumulation and film break down.**



**Fig. 12. Falling film profile at different time steps (Film Reynolds No= 1250 & S = 6.4).**

parameters. Also, for the tube spacing9.5mm the overall thickness decreases as compared to tube spacing 6.4mm. This happens due to gaining of more inertia by free falling of fluid and gravitation attraction due to greater spacing between tubes. At high film Reynolds number ($Re_f$= 1250) and intertube spacing 9.5mm waviness appears in the flowing fluid.

It is observed that the behavior of film thickness at lower Reynolds number ($Re_f$ = 650) is irregular in nature; the thickness decreases and the film breaks near the middle of the circumferential position ($90^0$ to $120^0$) of the tube (shown in Fig. 11.)

At low Reynolds number, the required momentum energy is insufficient to overcome the adhesive forces and surface tension acting on the fluid, hence the velocity gets reduced and mass accumulation starts. After sufficient mass accumulation, when the gravitational attraction force is enough to overcome the flow resisting forces, the flow suddenly begins and there is a tendency of breaks in film appearing. This discontinuity has also been also shown when the tube diameter is increased to 25.05mm. Abraham and Mani (2015) also concluded in their investigation that at low Reynolds numbers, formation of film thickness exhibits an abnormal behavior.

In our simulations, it is seen that the liquid film at tube spacing 3.2mm and at 6.4mm with low Reynolds number ($Re_f$ = 650) does not show streamlined flow. This fact has also been corroborated by Kocamustafaogullari and Chen (1988) who showed analytically that the effect becomes irrelevant when film Reynolds number is kept below $Re_f$ = 800. At lower Reynolds number viscous and gravity forces balance the inertia force. The film thickness behaves in an abrupt manner at higher film Reynolds ($Re_f$ = 1250) and when liquid goes to the lower side of the tube, the uniformity of thickness is lost and waviness appears in the flow.

### 4.3. Transient Flow Analysis

Film formation around the tube surface is a transient process and it varies with time. The flow data is captured at different time steps to visualize the film formation in different stages of flow (Fig. 12).

Observations are recorded for four different circumferential locations along the tube surface with film Reynolds number = 1250 and keeping the intertube spacing at 6.4mm. In stage-I, the liquid falls freely on the impingement zone of the tube surface making a thick film at that particular section. In this free fall condition, the liquid starts moving downward, the impingement zone is

covered with liquid and it continues to move downward along the tube surface with increasing velocity. In the next stage i.e. stage- II the liquid film covers most of the circumferential surface of the tube. It continues to flow to cover the entire surface in stage-III and leaves the contact surface of the upper tube. Moving on, a fully developed flow is visible in the last stage i.e. stage-IV and then the continuous column mode of flow is observed.

The velocity profile around the circumference of the outer surface of the upper tube is shown in Fig. 13. The falling liquid velocity gets its maximum value at a location where the film thickness approaches its minimum value and hence the law of mass conservation is justified.

Pathlines of flowing water are also captured on the upper surface of the tube in the range of 0º to 40º to show the flow characteristics clearly and it is depicted in Fig. 14. These flow visualizations are very insightful in understanding the flow behavior of liquid falling film on horizontal falling film tubular heat exchanger.
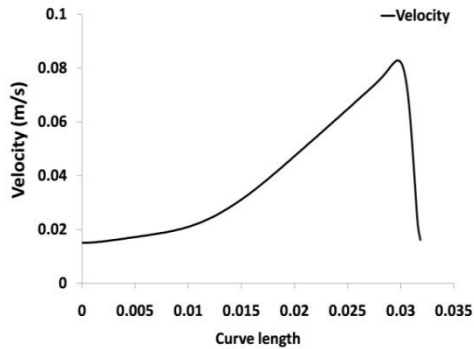


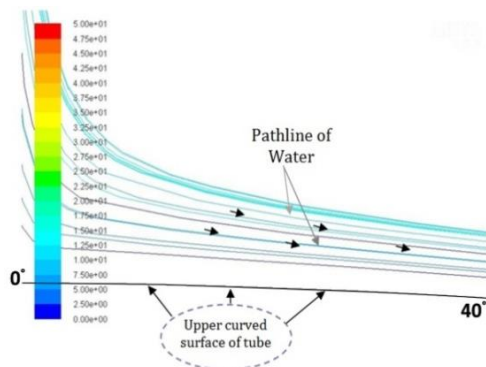**Fig. 13. Velocity profile around the circumference of the tube.**



**Fig. 14. Pathlines of falling film.**

## 5.  CONCLUSION

The falling film thickness is closely predicted by the present numerical simulation and it is demonstrated that the adopted simulation technique is capable of capturing the transient film formation process. The adiabatic case is modeled in absence of heat transfer. It is concluded that the film

thickness variation around the tube strongly depends upon the film Reynolds number and the intertube spacing. At very low film Reynolds numbers and small intertube spacing, the film thickness varies in an abrupt and unpredictable manner. However, this behavior may be attributed to the two-dimensional simulation of a complex three-dimensional phenomenon. The minimum thickness is achieved in the circumferential range of $110^0$ to $140^0$. This range is very critical for initiation of dry patch formation. It is also observed that the film thickness continuously increases with Reynolds number. When the Reynolds number increases, the location of minimum film thickness is shifted slightly towards the lower stagnation point of the tube. The peripheral film velocity increases continuously till attainment of minimum film thickness and then it increases slightly till the lowest circumferential position on the tube.

## REFERENCES

Abraham, R. and A. Mani (2015). Heat transfer characteristics in horizontal tube bundles for falling film evaporation in multi-effect desalination system. *Desalination* 375, 129-137.

Anglart, H. (2015). Dry patch formation in diabatic annular two-phase flows. *Journal of Power Technologies* 94(5), 85-95.

Armbruster, R. and J. Mitrovic (1998). Evaporative cooling of a falling water film on horizontal tubes. *Experimental Thermal and Fluid Science* 18(3), 183-194.

Chen, J., R. Zhang and R. Niu (2015). Numerical simulation of horizontal tube bundle falling film flow pattern transformation. *Renewable Energy* 73, 62-68. (Jingdong)

Christians, M. and J. R. Thome (2012). Falling film evaporation on enhanced tubes, part 1: Experimental results for pool boiling, onset-of-dryout and falling film evaporation. *International Journal of Refrigeration* 35(2), 300-312.

Desevaux, P., D. Homescu, P. K. Panday and J. P. Prenel (2002). Interface measurement technique for liquid film flowing inside small grooves by laser induced fluorescence. *Applied Thermal Engineering* 22(5), 521-534.

Dukler, A. E. (1952). Characteristics of flow in falling liquid film. In Proceeding of Chemical engineering progress symposium series 1952 48(11), 557-563.

Gstoehl, D., J. F. Roques, P. Crisinel and J. R. Thome (2004). Measurement of falling film thickness around a horizontal tube using a laser measurement technique. *Heat Transfer Engineering* 25(8), 28-34.

Hou, H., Q. Bi, H. Ma and G. Wu (2012). Distribution characteristics of falling film thickness around a horizontal tube.

*Desalination* 285, 393-398.

Ji, W. T., C. Y. Zhao, D. C. Zhang, S. Yoshioka, Y. L. He and W. Q. Tao (2016). Effect of vapor flow on the falling film evaporation of R134a outside a horizontal tube bundle. International *Journal of Heat and Mass Transfer* 92, 1171-1181.

Kocamustafaogullari, G. and I. Y. Chen (1988). Falling film heat transfer analysis on a bank of horizontal tube evaporator. *AIChE Journal* 34(9), 1539-1549.

Lee, Y. T., S. Hong, C. Dang, L. H. Chien, L. W. Chang and A. S. Yang (2019). Heat transfer characteristics of obliquely dispensed evaporating falling films on an elliptic tube. *International Journal of Heat and Mass Transfer* 132, 238-248.

Nusselt, W. (1916). Die oberflachenkondensation des wasserdamphes. VDI-Zs, 60, 541.

Ribatski, G. and J. R. Thome (2007). Experimental study on the onset of local dryout in an evaporating falling film on horizontal plain tubes. *Experimental Thermal and Fluid Science* 31(6), 483-493.

Rogers, J. T. and S. S. Goindi (1989). Experimental laminar falling film heat transfer coefficients on a large diameter horizontal tube. *The Canadian Journal of Chemical Engineering* 67(4), 560-568.

Wang, X., M. He, H. Fan and Y. Zhang (2009). Measurement of falling film thickness around a horizontal tube using laser-induced fluorescence technique. In Journal of Physics: Conference Series 147(1), p. 012039. IOP Publishing.

Wang, X., P. S. Hrnjak, S. Elbel, A. M. Jacobi and M. He (2010). Flow patterns and mode transitions for falling-film on flat tubes. In: International Refrigeration and Air Conditioning, School of Mechanical Engineering: Purdue University.

Wunder, F., S. Enders and R. Semiat (2017). Numerical simulation of heat transfer in a horizontal falling film evaporator of multiple-effect distillation. *Desalination* 401, 206-229.

Zhang, J. T., B. X. Wang and X. F. Peng (2000). Falling liquid film thickness measurement by an optical-electronic method. *Review of Scientific Instruments* 71(4), 1883-1886.